


Nonoxidative methane coupling in a micro-DBD with enhanced secondary electron emission

Nima Pourali¹  | Pradeep Lamichhane¹ | Volker Hessel^{1,2} | Evgeny V. Rebrov^{1,3}

¹School of Engineering, University of Warwick, Coventry, West Midland, UK

²School of Chemical Engineering and Advanced Materials, University of Adelaide, Adelaide, Australia

³Department of Chemical Engineering and Chemistry, Eindhoven University of Technology, Eindhoven, The Netherlands

Correspondence

Nima Pourali, School of Engineering, University of Warwick, Coventry CV4 7AL, UK.

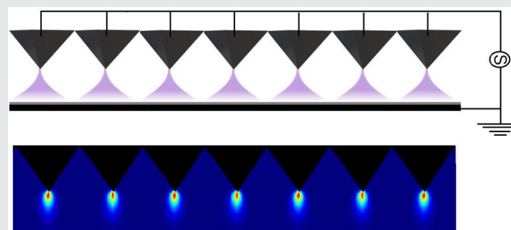
Email: n.pourali86@gmail.com and Nima.Pourali@warwick.ac.uk

Funding information

H2020 European Research Council, Grant/Award Number: 810182

Abstract

The conversion of methane into transportable and storable materials is crucial in the petrochemical sector. In this study, a specially constructed AC-driven dielectric barrier discharge (DBD) that has charge injector pyramids on one of the electrodes and runs at ambient temperature and pressure was used to evaluate noncatalytic methane conversion. The obtained result was compared with the traditional flat electrode DBD. It was discovered that the product selectivity in direct nonoxidative methane conversion depended on the discharge conditions. Pyramid electrode plasma sources convert methane up to 50% more than flat electrode plasma due to the appearance of more microdischarges. Pyramid electrode plasma generally has a greater production efficiency than flat electrode plasma, while requiring more operational power. The turn-key solutions offered by the sustainable methane coupling method discussed here may be advantageous for the long-term small-scale ethylene exploration scenario.



KEYWORDS

charge injection, DBD plasma, energy efficiency, methane coupling, secondary emission

1 | INTRODUCTION

Methane found by Alessandro Volta in the muddy waters of Lake Maggiore in 1776^[1] is one of the most important chemical feedstocks used in the chemical industry to synthesize high-value products. It is cost-effective natural gas as a fuel because of the high hydrogen-to-carbon ratio and an essential raw material for the creation of polyethylene, plastic, detergent, synthetic rubber, and fiber.^[2,3] But, until now, most of the available resources

are still underutilized due to the requirement of sophisticated storage systems and high transportation costs. It ranks right behind carbon dioxide as the most common anthropogenic greenhouse gas, 25 times more atmospheric heat is trapped by it than by carbon dioxide.^[4] In the petrochemical industry, methane conversion into products that can be stored and transported is, therefore, essential.^[5] Numerous academics are interested in methane transformation options as a means of reducing reliance on crude oil. In terms of methane conversion technology, there

This is an open access article under the terms of the Creative Commons Attribution License, which permits use, distribution and reproduction in any medium, provided the original work is properly cited.

© 2023 The Authors. *Plasma Processes and Polymers* published by Wiley-VCH GmbH.

are two basic approaches. They are conversions, both direct and indirect.^[6] Indirect conversion is similar to the steam reformation technique used in the ammonia synthesis business (Haber–Bosch process),^[7] while direct conversion involves both oxidative and nonoxidative conversion.

Some of the earliest techniques in methane conversion technology were steam reformation (methane conversion with water), dry reformation (methane conversion with carbon dioxide), and bireformation (methane conversion using both steam and dry reformation).^[8] The main disadvantage of all these reforming processes is the higher temperature carbon deposition.^[9] Because of the significant volumes of unneeded carbon dioxide,^[10] carbon monoxide, and coke are emitted into the environment even though this process employs a sustainable energy source. We are always enthusiastic for carbon-free methane activation and coupling techniques.

A large number of research has been already performed on sustainable nonoxidative direct methane conversion methods like photo-catalysis,^[11] electrocatalysis,^[12] biocatalysis,^[13] and plasma-catalysis^[14] are acknowledged as an alternative to the thermal process during the last few decades. Free radicals (such the OH radicals) are produced in photo-catalysis as a result of electron–hole pairs created by photon energy. These free radicals can then undergo further reactions. This method is economical, cost-effective, and does not produce any more pollution. However, it takes a long period and has a low methane coupling efficiency.^[11] Similar to this, in electrocatalysis, electrons are transported directly between two terminals with higher and lower potentials. An oxidation process occurs at the anode, and a reduction reaction occurs at the cathode. In the electrocatalytic methane conversion method, reaction activity and selectivity can be adjusted by varying the applied potentials without heating the catalyst. However, this method also has weak catalyst electro-conductivity and low faradaic efficiency.^[12] Heat is a waste byproduct at the same time. Biocatalysis, which uses enzymes of bacteria as catalysts for redox reactions, is another environmentally friendly technique. It is also extremely efficient and selective. The drawbacks of the biocatalytic approach include a lack of design-ability and stability, a lack of ready-to-use bio-catalysts, and the fact that biocatalysts become inactive in organic solvents, at high temperatures, and at extreme pH levels.^[13]

To address these issues, nonthermal plasma (NTP) generated by dielectric barrier discharge (DBD) has been viewed as a potential and developing alternative that enables methane activation at low temperatures and ambient pressure.^[15] In contrast to thermal plasma, NTPs only produce highly energetic electrons and reactive species while maintaining a low gas kinetic

temperature. When molecules in NTPs are activated by vibrational and electronic excitations, which causes their dissociation, a variety of chemical processes take place. The use of NTP for the methane activation-based synthesis of chemicals and fuels has gained popularity recently.^[15–17] Recently, we have shown theoretically and computationally that dielectric barrier discharges with charge injection points have further practical benefits.^[18,19] Following that, in this experimental study, we explore methane conversion in an AC-driven charge injector DBD and compare the results to the usual flat electrode DBD plasma. The sharp points on the electrodes of this specific DBD produce a high-rate secondary electron emission due to the high strength of the local electric field, which might eventually boost methane activation and energy efficiency of the process.

2 | EXPERIMENTAL SETUP AND METHODOLOGY

The interior of the plasma reactor used in this experiment is shown in Figure 1. To avoid the arcing between the edge of the high voltage (HV) electrode and the ground electrode, the circular disc of the ground electrode covered by the dielectric layer was chosen wider than the HV electrode. The diameter of the ground electrode disc is 23 mm but the HV disc has a diameter of 22 mm. Both electrodes were positioned inside the cylindrical quartz tube at adjustable distances from each other. When electrodes are of the same size and they are in contact with the quartz tube, due to the surface charge accumulation on the inner side of the quartz tube, plasma makes a quick transition to the arc regime. Therefore, to tackle this problem the sizes of the electrodes were chosen smaller than the inner tube diameter of 24 mm and also different from each other. The dielectric layer covering the ground electrode is a 0.2-mm thick mica film, which has dielectric strength of 25 kV/mm and can stand to a temperature over 500°C. The temperature of the electrode was maintained at 20°C with water cooling. The experimental set-up was presented in our previous work.^[20] A 400 pF external capacitor was connected to the ground line to monitor the generated electric charges (Q) in the plasma. A high-voltage power generator (G2000 Redline Technologies) was used as an electrical power source that generates different amplitudes of the sinusoidal wave with various frequencies. A fixed frequency of 68 kHz was applied to the plasma reactor. Industrial pure methane gas (99.999 vol %) was used as a main working gas and a Bronkhorst mass flow controller was used to regulate the methane flow in the reactor.

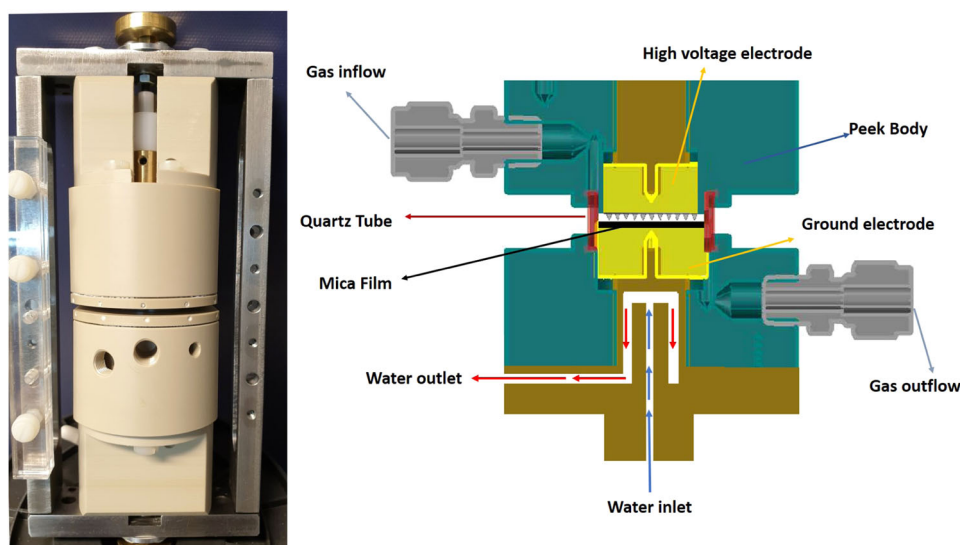


FIGURE 1 Structure of the plasma reactor and its interior design.

A Rogowski coil (Pearson 6600) and 1000× High Voltage Probe (Tektronix P6015A) were utilized to measure the current and voltage, respectively. The voltage and current were recorded by oscilloscope (pico-scope 3000 series from pico-tec). The Princeton Instruments FERGIE Fiber Optic Spectrometer (FER-SCI-1024BX-UR) was utilized to detect the light emission profile from the plasma with the help of optical fiber at perpendicularly 5 mm far from the window of the reactor. This optical emission spectrometer (OES) is equipped with a grating of 1200 lines/mm, and a 25 mm slit to provide coverage over the range 200–1100 nm with ≈ 0.26 nm resolution. A back-illuminated, integrated, deep-cooled (-55°C , 1024×256 charge-coupled device) array was used for extremely low noise. The outlet of the plasma cell was connected to a two-channel (Rt-QS-BOND (RESTEC) and SH-Massive 5A (SHIMADZU)) gas chromatography (GC) (SHIMADZU 2010 Pro) with a thermal conductivity detector (TCD) and a flame ionization detector (FID) was used to examine the outlet gaseous products.

We used an identical setup in two types of HV electrodes, one is flat electrode DBD and another is pyramid electrode DBD. A schematic of the design for the flat electrode is shown in Figure 2a. The flat HV electrode has a uniform surface thus it produces a uniform electric field over all surfaces which is represented in Figure 2b. A schematic of the pyramid electrode is shown in Figure 2c. Free electrons in a metal conductor desire to accumulate in sharp points away from the center of the metal. This means charge density is high in sharp points. The higher surface charge density produces a higher electric field, so the

electric field is stronger at the tip of the pyramid electrode as shown in Figure 2d. A stronger electric field generates a high rate of secondary electron emission, so these sharp points are named charge injectors. An array of 160 uniform pyramids was engraved for establishing charge injection phenomena. A photograph of the pyramid electrode is shown in Figure 2e. Dimensions of the pyramid and their separations are shown in Figure 2f,g. Each pyramid base has an area of 1mm^2 , and their heights and separation distances are fixed at 1 and 0.5 mm, respectively. Additionally, the curvature radius of the pyramid tip was chosen to be $25\ \mu\text{m}$ because there is no infinite sharp point in reality.

Methane conversion was estimated by Equation (7)^[21]:

$$\text{CH}_4 \text{ conversion } [\%] = \frac{\text{Converted CH}_4 \text{ flow}}{\text{Inlet CH}_4 \text{ flow}} \times 100\% \quad (1)$$

Also, the CH_4 conversion efficiency in millimoles per kilowatt hour [mMol/kWh] was estimated by using Equation (2).

$$\text{Conversion efficiency} = \frac{\text{Converted CH}_4 \left[\frac{\text{mMoles}}{\text{hour}} \right]}{\text{Power [kilowatt]}} \quad (2)$$

Similarly, the selectivity and production efficiency of ethane (C_2H_6) and ethylene (C_2H_4) were estimated by using the following Equations (3) and (4), respectively^[22]:

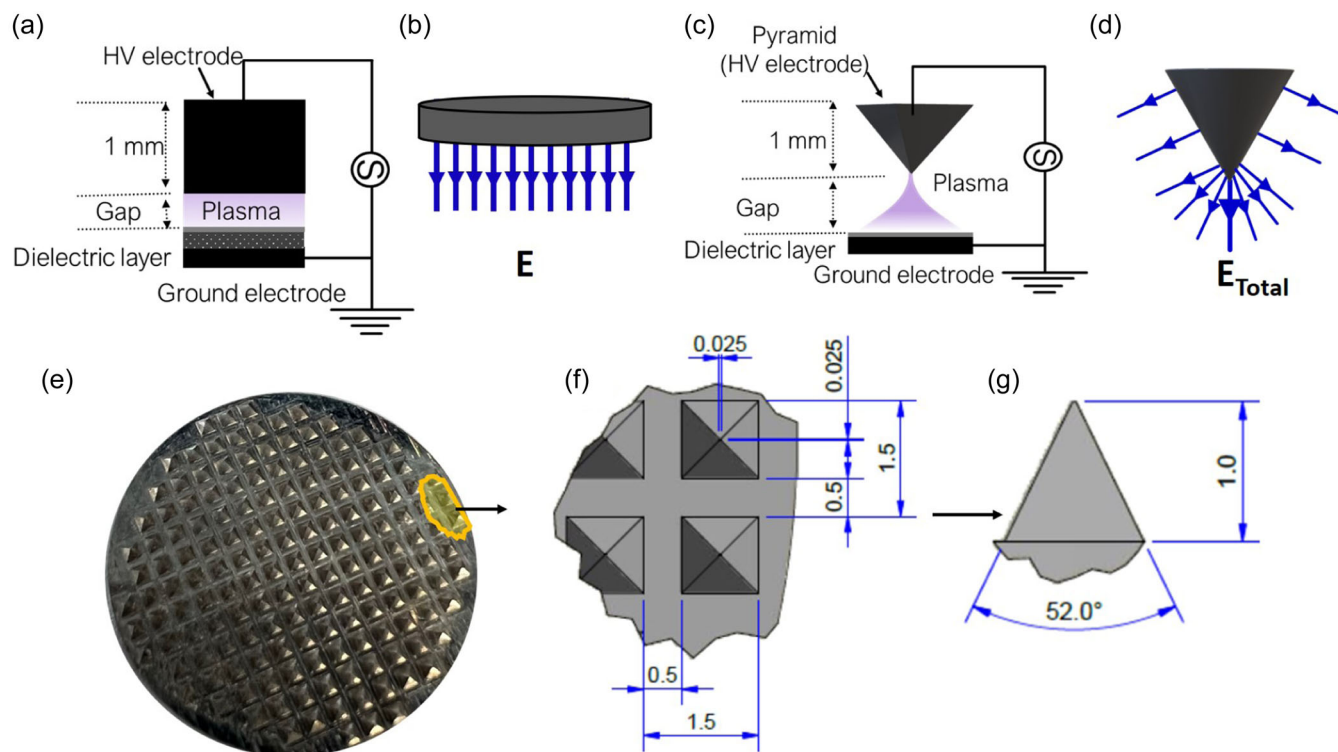


FIGURE 2 (a) Schematic of flat electrode dielectric barrier discharge. (b) Representation of electric field in flat electrode dielectric barrier discharge. (c) Schematic of Pyramid electrode dielectric barrier discharge. (d) Illustration of the electric field in pyramid electrode dielectric barrier discharge. (e) Photograph of pyramid array high voltage electrode. (f) Horizontal and (g) vertical view of pyramids and their dimensions.

$$C_2H_y \text{ selectivity} = 2 \times \left[\frac{C_2H_y \text{ formation rate}}{CH_4 \text{ conversion rate}} \right] \times 100\%, \quad (3)$$

$$C_2H_y \text{ production efficiency} = \frac{\text{Produced } C_2H_y \left[\frac{\text{mMoles}}{\text{hour}} \right]}{\text{Power [kilowatt]}}. \quad (4)$$

In methane plasma carbon disposition and coke formation is not avoidable. To reflect the coke formation and the C atom balance, the carbon lack is calculated by the following equation:

$$C_{\text{lack}} = \left(\frac{F_{\text{out}}}{[CH_4] \cdot F_{\text{in}}} - 1 - ([CH_4] + 2[C_2H_2] + 2[C_2H_4] + 2[C_2H_6] + 3[C_3H_6] + 3[C_3H_8]) \cdot \frac{F_{\text{out}}}{[CH_4] \cdot F_{\text{in}}} \right) \cdot 100\%, \quad (5)$$

where $[...]\text{in}$ and $[...]\text{out}$ are inlet and outlet concentrations and F_{in} and F_{out} are the inlet and outlet flow rates, respectively. The carbon lack takes into account the

carbon deposition and carbon loss due to the unidentified products by GC. Coke deposition affects the performance of reactors in methane plasma processes. The carbon deposition over the dielectric layer (Mica film) changes the performance of the reactors due to the change in the net dielectric constant of the barrier. Therefore, acquiring data in each experiment was carried out 15 min after plasma ignition. Also, the coke inside the reactor was completely cleaned before running any experiment with new conditions.

3 | RESULTS

3.1 | Electrical properties

Figure 3a depicts the current–voltage waveform of a typical AC-driven plasma source. At both rising and descending portions of the applied voltage, there are many current peaks for a duration of a few microseconds to nanoseconds. Both plasma sources have identical discharge patterns, but the plasma of the pyramid electrode DBD has higher current peaks. The accumulation of wall charge (Q) during the positive half cycle of the applied voltage is diminished at the negative half

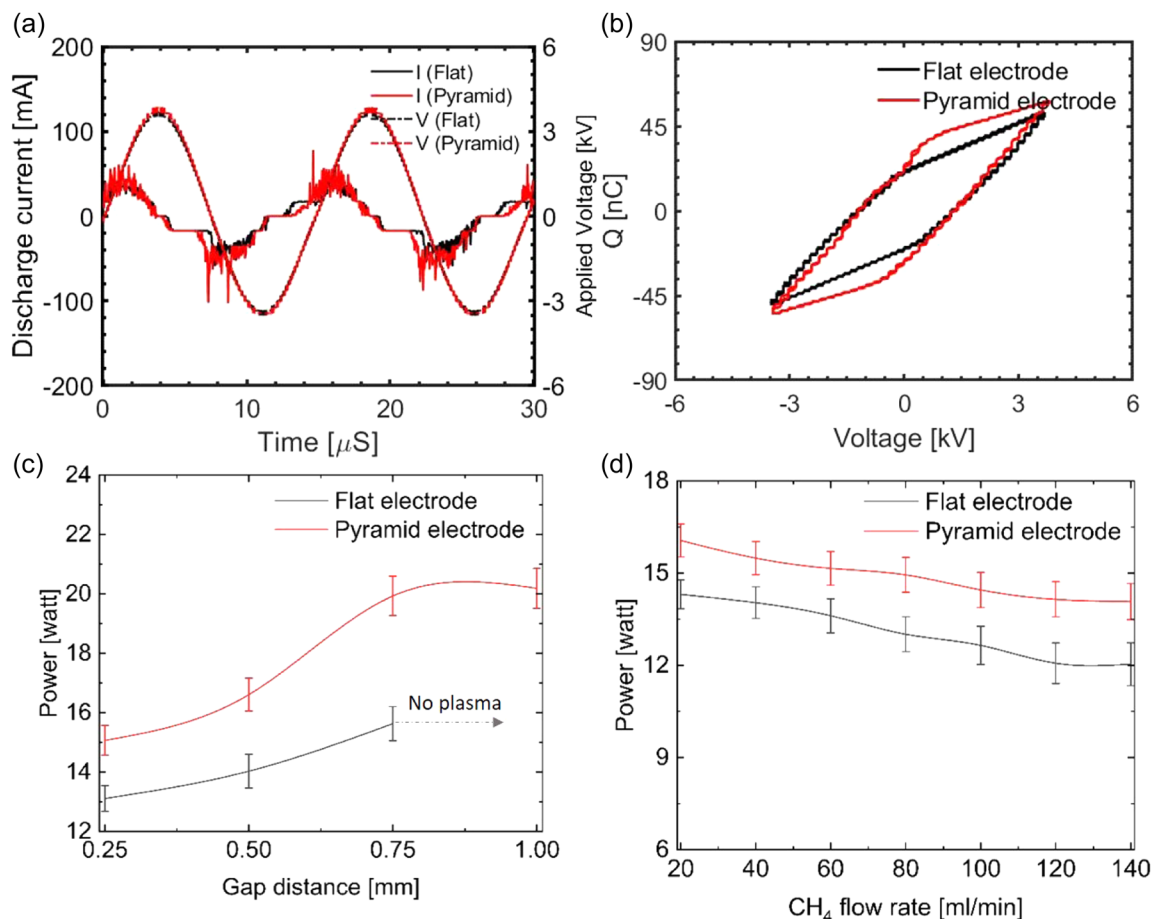


FIGURE 3 Comparison of electric current and voltage profiles (a) and Lissajous plots (b) of flat and pyramid electrode reactors at gap distance of 0.5 mm and flow rate of 20 mL/min. Also, comparison of power consumed by two reactors at different gap distances (c) and gas flows (d). The input voltage and frequency are fixed at $V_{pp} = 6.5$ kV and 68 kHz, respectively.

cycle of applied voltage. After the positive and negative discharges, the amount of wall charge decreases sharply with time, leading to an increase in gas resistance. The net charge transported over the course of a complete cycle is zero; thus, the $Q-V$ plot (Lissajous figure) must be closed and it resembles a parallelogram as shown in Figure 3b. The area of the closed loop gives the total power required for plasma as is given in Equation (6). It is clearly seen that area of the Lissajous loop for the pyramid electrode is wider than that of the flat electrode which is due to the larger current peaks (microdischarges) in the pyramid electrode at the same applied voltage.

$$P = \frac{1}{T} \int_0^T IV dt = \frac{1}{T} \int_0^T V dQ. \quad (6)$$

Comparing electric power consumed by flat and pyramid electrode DBDs for different feedstock methane flow rates and for different discharge gaps reveals that for each condition of flow rate and discharge gap the

pyramid electrode DBD consumes more power in comparison with flat electrode DBD. For discharge gaps bigger than 0.75 mm applying a voltage $V_{pp} = 6.5$ kV does not create a plasma in the flat electrode DBD, while a stronger plasma is observed in the pyramid electrode reactor for this applied voltage due to the high electric field at the tip of pyramids. In the bigger discharge gaps, the volume of gas present in the plasma region is high, so the number of molecules going under the ionization process due to collision with energetic electrons increases, and more charge carriers (ions and electrons) are produced. Subsequently, more electrons receive electric energy from the background electric field. This phenomenon increases the electric current and consumed power. However, the increase in the discharge gap in fixed applied voltage leads to a decrease in the intensity of the background electric field between electrodes, so the energy of electrons interacting with the electric field decrease and they do not have sufficient energy to ionize molecules in more big gaps, which this happens for flat electrode DBD in discharge gaps above

0.75 mm and for pyramid electrode DBD in discharge gaps above 1.25 mm. The difference between the consumed powers of flat and pyramid electrode DBDs and especially their breakdown difference in larger gaps are related to enhanced secondary electron emission in the tip of pyramids. According to Coulomb's law, around the sharp points of a metal connected to high voltage the electric field is higher. A higher electric field delivers more energy to electrons close to sharp points. Also, when an electric field is high the rate of secondary emission increases because ions colliding with sharp points have more energy due to strong interaction with the electric field. Increasing the flow rate at the fixed voltage and discharge gap decreases the residence time of background gas molecules and shortens the time that they spend in the plasma region. Therefore, the cumulative ionization probability of molecules decreases, and charged particles (ions and electrons) are produced at a lower rate in the discharge region. The latter makes the electric current, given by the flux of charged particles, become small, and the consumed power calculated from Equation (6) shows a decrease in value by the increase in the flow rate of methane.

Figure 4 compares power against the voltage for two reactors and shows how consumed power changes by voltage for each reactor. Plasma ignition in each reactor happens in different minimum powers and also maximum powers that each reactor can stand, without going to arc regime, are not the same. Note that the electric field intensity is governed by the applied voltage. Also, according to Equation (6), plasma power is a dependent parameter that is determined by the applied voltage and the electric charge created in the plasma. The reactors with the same power in different applied voltages have different reduced electric fields in the discharge gaps. Therefore the rate of ionization, and species collision, and charged species densities will be different and they follow different reaction mechanism pathways. The

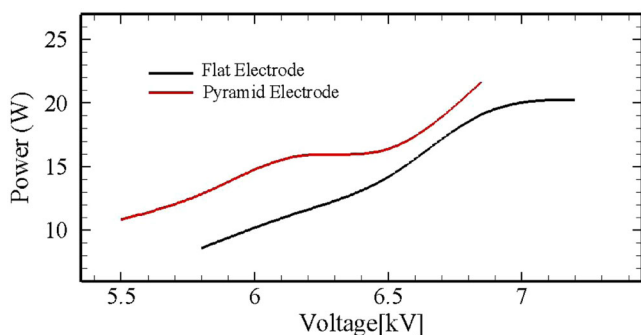


FIGURE 4 The consumed power as a function of voltage in the default flow rate of 20 mL/min, discharge gap of 0.5 mm, and frequency of 68 kHz.

production rate of charged species depends on the strength of the electric field established in the discharge gap and on the ionization energy of neutral molecules of background gases. The higher power at an applied voltage means that the strength of the electric field in the discharge gap is higher which is established in the pyramid electrode reactor by sharp points.

3.2 | Optical emission spectroscopy

For the detection of numerous reactive and excited species in the plasma phase, OES is a widely used, quick, practical, and straightforward method.^[23] The evolution of the H and CH species in postdischarge clearly represents the conversion of methane in the plasma. Figure 5 shows the OES in the 300–700 nm range. There are peak of CH(C-X) due to the transition $C^2\Sigma^+ \rightarrow X^2\Pi$ at 314.3 nm and peak of CH(B-X) due to the transition of $B^2\Sigma \rightarrow X^2\Pi$ at 388.9 nm.^[24,25] They are not predominantly seen in flat electrode DBD plasma. Besides this, the most dominant emission peaks that are available in both plasmas are CH(A-X) due to the transition $A^2\Delta \rightarrow X^2\Pi$ at 431.5 nm.^[24,26] Hydrogen emission lines such as H_β (Balmer $n = 4 \rightarrow 2$) at 486.1 nm, H_α (Balmer $n = 3 \rightarrow 2$) at 656.3, and H_2 (Fulcher $d^3\Pi_u^- \rightarrow a^3\Sigma_g^+$) at 628.2 nm also appeared clearly.^[24,26,27] In addition, carbon emission lines of C_2 such as Swan $d^3\Pi_g \rightarrow a^3\Pi_u$ at 516.2 nm and Swan $d^3\Pi_g \rightarrow a^3\Pi_u$ at 563.2 nm are also appeared.^[26,27] Based on pilot observations on OES, the pyramid electrode appears to stimulate more methane in the gas phase than the flat electrode DBD plasma does. We simulated OES of CH(A-X) for both flat electrode DBD and pyramid electrode DBD in LIFBASE or

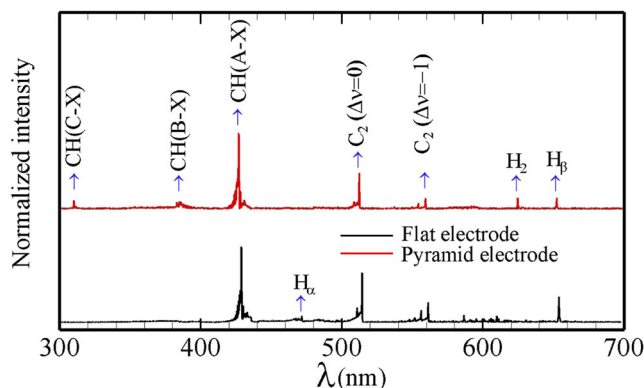


FIGURE 5 Comparison of the optical emission spectrum of methane plasmas generated by the flat electrode and pyramid electrode dielectric barrier discharges (applied voltage: $V_{pp} = 6.5$ kV, methane flow rate 20 mL/min, electrode separation = 0.75 mm, frequency = 68 kHz).

Pghoher to calculate the rotational and vibrational temperatures through fitting them to the experimental spectrum, as shown in Figure 6. The rotational temperature for pyramid electrode DBD is higher than that of flat electrode DBD, while the vibrational temperatures of both reactors are very close to each other, slightly higher for flat DBD. High rotational temperature reflects more gas heating and high translational temperature due to a strong correlation between them. The high heating at the tip of the pyramids causes a higher rotational temperature in the pyramid electrode DBD. High electric fields produce more heating due to the joule heating,^[20] so near the sharp points there is more gas heating which results in more increase in rotational temperature. In pyramid electrode DBD, near the sharp point ions are accelerated due to the high intensity of the electric field and their drift velocity is high. These fast-moving ions collide energetically with background gas molecules that have comparable masses with them. It causes the background molecules to move at a higher speed too. Therefore, near the sharp point, the temperature of the background gas (translational temperature) increases, and the gas heats more. Since there is a close correlation between the rotational and translation temperatures of a

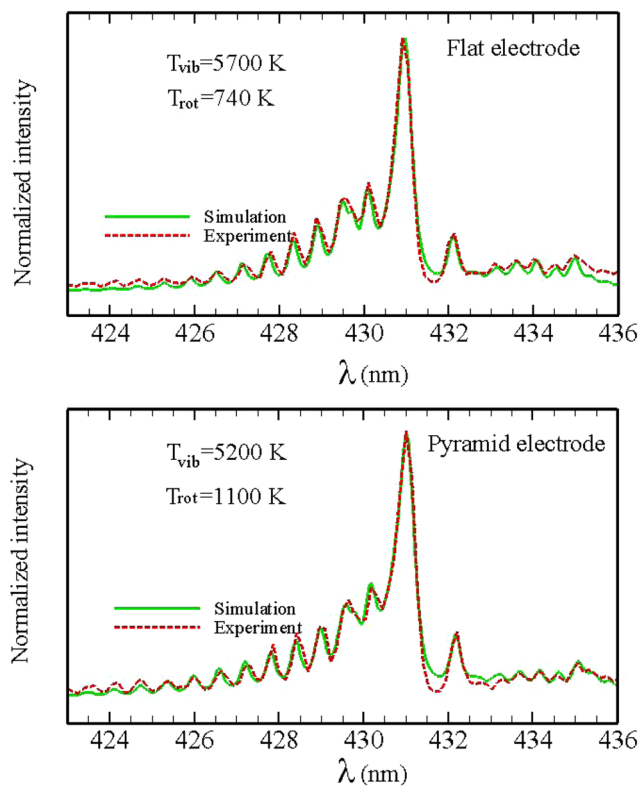


FIGURE 6 Rotational and vibrational temperatures calculated from CH(A-X) peak in flat and pyramid electrode dielectric barrier discharges. The conditions are the same as in Figure 5.

background gas, the rotational temperature is also high in pyramid electrode DBD.

3.3 | The methane conversion and selectivity of products

The variation of methane conversion with an increase in gap distance between two electrodes and with an increase in methane flow rate and fixed flow rate and discharge gap are shown in Figures 7a and 7b, respectively. The obtained results for flat electrode and pyramid electrode DBDs are compared. The gap distance between the HV electrode and the ground directly affects the electric field. In this experiment, the maximum methane

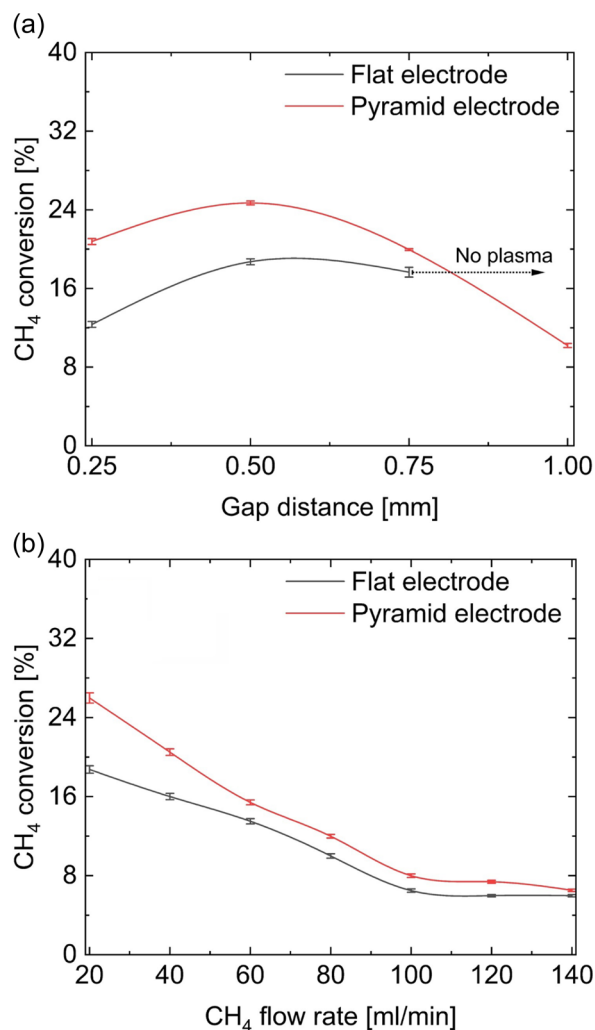


FIGURE 7 Variations of methane conversion (a) by increasing gap distance at a constant methane flow rate of 20 mL/min and also variations of methane conversion (b) by increasing the methane flow rate at a constant gap distance of 0.5 mm in flat and pyramid electrode dielectric barrier discharges. The applied voltage and frequency are fixed at $V_{pp} = 6.5$ kV and $f = 68$ kHz, respectively.

conversion was obtained at a gap distance of 0.5 mm in both plasma sources, but the pyramid electrode has more than 10% conversion as compared to the flat electrode DBD. Maximum 24% methane was converted by pyramid DBD at an applied voltage of $V_{pp} = 6.5$ kV, gap distance of 0.5 mm. According to Figure 7b, CH_4 conversion decrease with an increase in CH_4 feeding rate in both reactors. Any change in the inlet flow rate changes the residence time of the reactor and the duration that species spends in the plasma reactor before going out. When the gas flow rate increases the residence time of the reactor decreases and molecules of background gas spend less time in the discharge region, as some of them leave the reactor without reacting with plasma species, so the conversion for both electrodes decreases by the increase of background gas flow rate.

Figure 8 illustrates the selectivity of different products and carbon lack in different inlet gas flow rates and discharge gaps for pyramid and flat electrode DBDs. In both reactors, in any flow rate condition, the dominant selectivity belongs to C_2H_2 . The carbon lack in the pyramid electrode is higher than the carbon lack in flat DBD. It decreases with the increase of the flow rate in both reactors. This means when the conversion is low the carbon lack is less (see Figure 7b). Flat electrode DBD

plasma has 15% more C_2H_6 selectivity but pyramid electrode plasma has approximately 10% more C_2H_4 selectivity. The selectivity of both C_2H_6 and C_2H_4 increase with the increase in flow rate. The plasma of the flat electrode DBD is more selective toward the C_2H_6 , whereas pyramid electrode plasma is more selective toward the C_2H_4 . The main reason for the change of selectivity from ethane to ethylene in the pyramid reactor is the dehydrogenation process. High heating at the tip of the pyramids due to a high electric field (joule heating) is the main reason for the dehydrogenation of ethane. Figures of selectivity in different discharge gaps for both reactors show that by decreasing gap size the selectivity of C_2H_6 increases and it becomes more selective than C_2H_4 .

3.4 | The energy efficiency of conversion and production

Comparison of energy efficiencies for the pyramid and flat electrode DBDs in different gap distance and flow rate conditions are carried out in Figure 9. At fixed voltage $V_{pp} = 6.5$ kV and different discharge gap conditions, the highest conversion energy efficiency for both

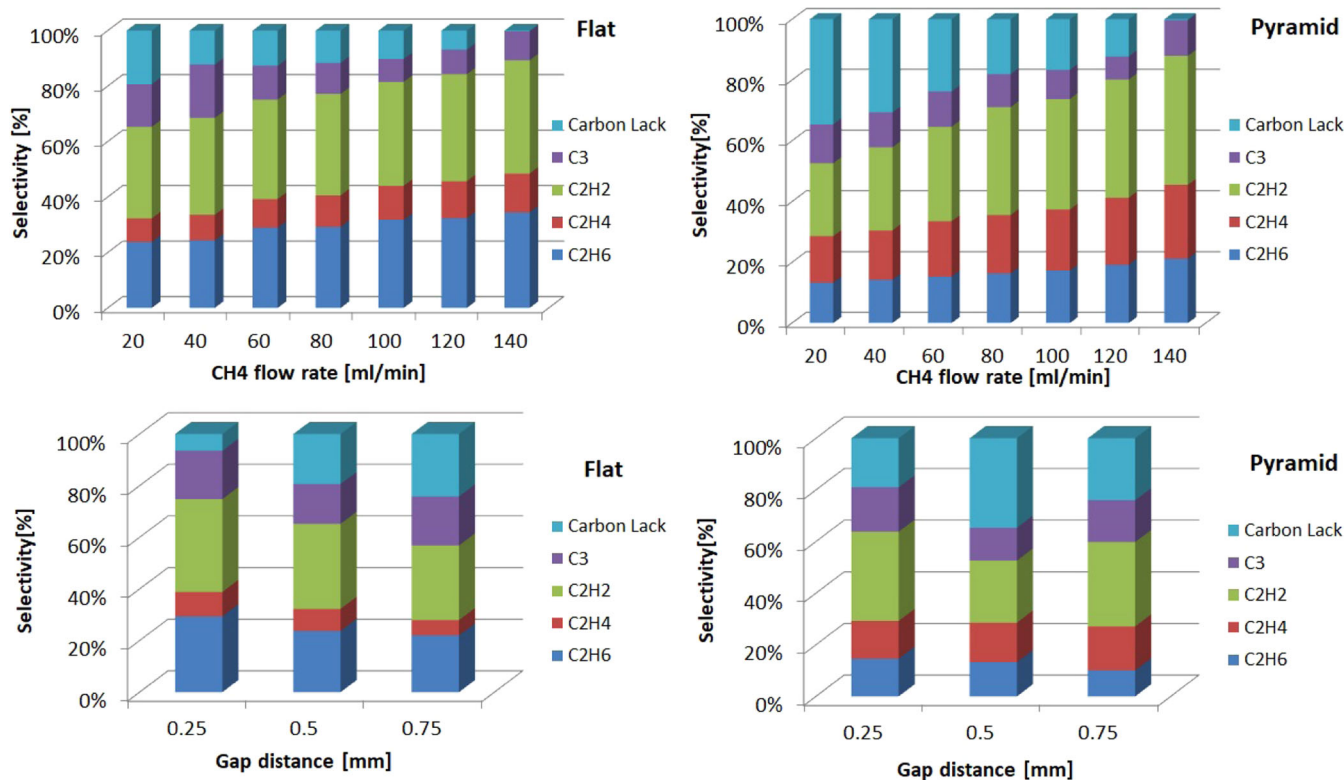


FIGURE 8 Variations of selectivities of products and carbon lack by changing gap distance and the methane flow rate in flat and pyramid electrode dielectric barrier discharges. The default parameters are the gap distance = 0.5 mm, methane flow rate = 20 mL/min, $V_{pp} = 6.5$ kV, and $f = 68$ kHz.

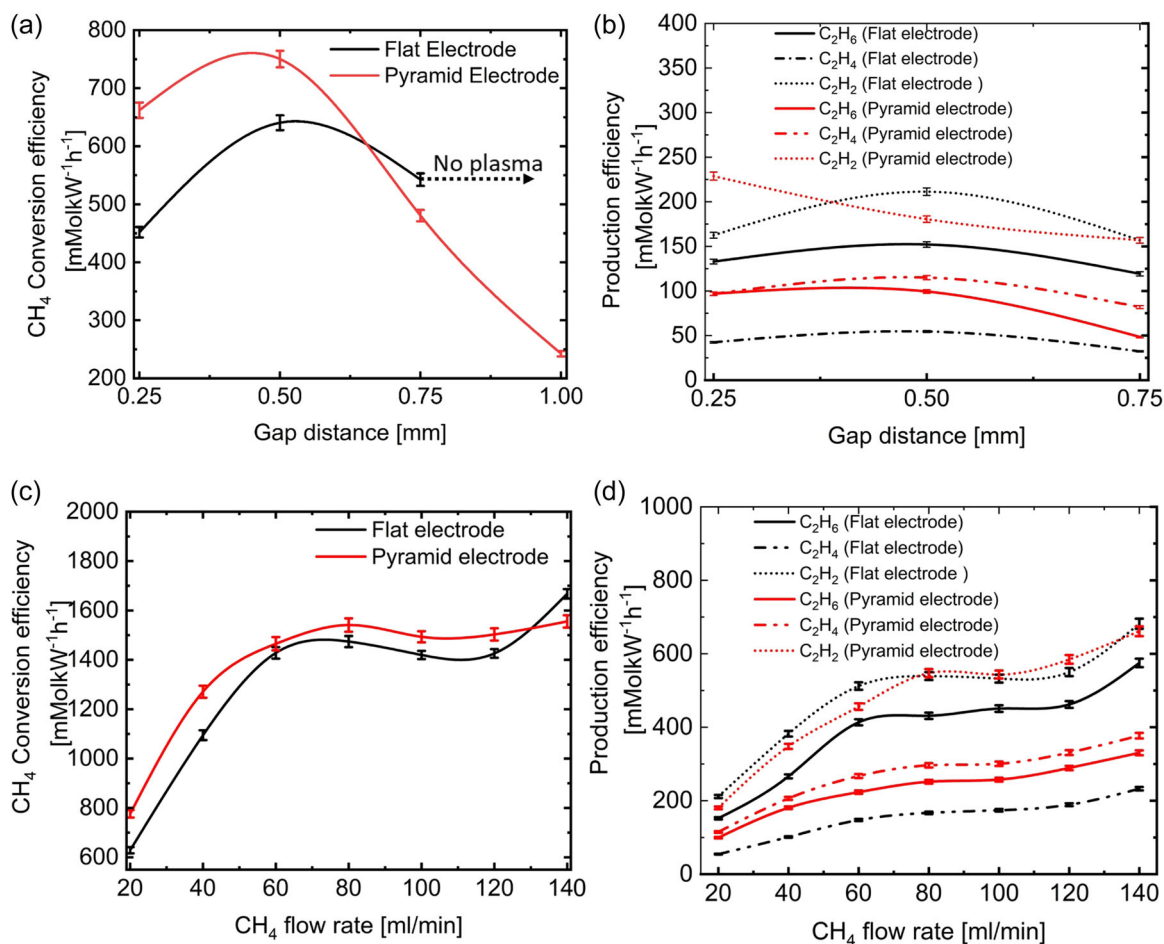


FIGURE 9 Variations of methane conversion efficiency (a) and production efficiency of different hydrocarbon products (b) by increasing gap distance at a constant methane flow rate of 20 mL/min and also variations of methane conversion efficiency (c) and production efficiency of different hydrocarbon products (d) by increasing the methane flow rate at a constant gap distance of 0.5 mm in flat and pyramid electrode dielectric barrier discharges. The applied voltage and frequency are fixed at $V_{pp} = 6.5$ kV and $f = 68$ kHz, respectively.

DBDs appears in the discharge gap of 0.5 mm. The conversion efficiency of pyramid electrode DBD is higher than that of flat electrode DBD for small gaps while by increasing the discharge gap from 0.5 to 0.75 mm energy efficiency of the pyramid becomes smaller than that of flat electrode DBD. For the gap of 1 mm there is no plasma formation in flat electrode DBD, but for pyramid DBD of this discharge gap, the conversion efficiency is in the lowest value. Production efficiency of ethane according to Figure 9b decreases with increasing discharge gap in pyramid electrode DBD while changing the discharge gap does not remarkably change the production efficiency of ethylene in this reactor. For the discharge gap of 0.5 mm in flat electrode DBD, the production efficiencies of produced species are slightly higher than those of other discharge gap conditions. Changes in flow rate in fixed voltage and constant discharge gap strongly changes conversion efficiency and production efficiencies. According to Figure 9c,d, with the increase of flow

rate from 20 mL/min quick growth in efficiencies happens, but increasing flow from 60 to 130 mL/min does not significantly change the conversion and production efficiencies. Conversion efficiency in pyramid electrode DBD is higher than Conversion efficiency in flat electrodes in all flow rates below the flow rate of 130 mL/min, but the flat DBD has higher conversion efficiency in flow rate above it. Comparing the production efficiencies in flat and pyramid DBDs reveals that the production efficiency of ethylene is higher than the efficiency of ethane in all flow rate ranges in the pyramid DBD while in flat electrode DBD it is reversed and ethane production is more efficient than ethylene production.

As mentioned before when the gas flow rate increases the residence time of the reactor decreases and molecules of background gas spend less time in the discharge region, so the ionization rate becomes small. It results in less electric charge production and the power (as a

function of electric charge) decreases (the denominator in Equation 2). Meantime, with the increase of flow rate the conversion also decreases because of the lower residence time (Numerator in Equation 2). These two opposite effects compete with each other to determine the energy efficiency of the conversion. The decrease in consumed power with the increase of flow rate is more vigorous than the decrease of conversion because with the increase of flow rate gas heating also decreases and the majority of delivered energy is channeled in the reaction processes, instead of momentum collisions. However, more increase in flow rate leads to more decrease in conversion, due to the reduction in delivered energy to gas, so the decrease in conversion and the power balance each other in a higher flow rate and result in a stable efficiency as the figure shows.

4 | DISCUSSION

Low-mass electrons in the plasma absorb the majority of the electric energy that is applied to it. The methane molecules are stimulated, ionized and dissociated when an energetic electron collides with them. Because of this, extraordinary chemical reactions can occur at normal pressures and temperatures.^[28,29] The generation of methyl radicals (CH_3), methylene radicals (CH_2), and methylidyne radicals (CH) in the plasma is mostly caused by the dissociation of CH_4 as a result of the energy-impact collision with an energetic electron. Methane coupling is dependent upon the concentration of plasma-generated radicals. Previous research has suggested that recombination reactions of CH_3 give rise to the saturated product C_2H_6 . At the same time, the production of unsaturated hydrocarbons such as C_2H_4 and C_2H_2 is mainly formed by the recombination process of CH_2 and CH , respectively. The change of higher selectivity between C_2H_6 and C_2H_4 in the reactors is carried out by the thermal dehydrogenation of C_2H_6 - C_2H_4 . Therefore, due to more heating in the pyramid electrode DBD the C_2H_4 has more selectivity than C_2H_6 .

Dielectric barrier discharge is sustained by secondary electron emission and/or field emission effects. The field emission effect appears when the discharge gap or surface imperfections are in scale size smaller than $10\ \mu\text{m}$ (electric field strength higher than $10^8\ \text{V/m}$). Therefore, in bigger discharge gaps the field emission effects are negligible and the most important factor of self-sustainability becomes the intensity of secondary electron emission from electrodes and reactor walls. In this situation, the gas breakdown voltage is governed by Paschen's equation, which takes into consideration Townsend processes, electron impact ionization in most

of the plasma and secondary electron emission from the electrodes and walls. The flux of the secondary electron emission is given by:

$$\Gamma_{\text{sec}} = \gamma \mu_i n_i \vec{E}, \quad (7)$$

where γ secondary emission is constant, μ_i is the mobility coefficient of the ion, and \vec{E} is the electric field. According to the above equation, around sharp points where there is a high-strength electric field, the secondary emission flux increases and an enhanced secondary emission effect appears. Also, the velocity of the ions ($\mu_i \vec{E}$), which controls the flow of secondary electron emission, is also dependent on the strength of the electric field. It is clear that around sharp points where the electric field is accumulated, the secondary emission process becomes stronger. These pointy edges are the charge injection parts.^[18,19] Additionally, the strong reduced-electric field (E/N_{gas}) because of the surface imperfections accelerates electrons and collides them aggressively with other species to create more reactive species and a reactive environment. It is noteworthy to mention that the pyramid electrode DBD presented in this work has been designed based on our previous computational research,^[18,19] where the effects of sharp points in DBD on the physics and chemistry of the plasma have been discussed in more detail.

Therefore, in fast-modulated plasmas with electrodes containing sharp points and with small discharge gaps, due to the increase in the reduced-electric field and high rate of secondary electron emission, the electron density, the electron temperature and the density of reactive species are higher. These lead to changes in the reaction mechanism, reaction pathways of producing the product species, the conversion rate, and energy efficiency of the conversion, as we predicted previously in references^[18,19] and as we observed here in the previous section of the paper.

5 | CONCLUSION

This paper gives a general outline of one-step, noncatalytic, nonoxidative direct methane coupling with an emphasis on ethylene. Due to the high intensity of the local electric field and the sharp points on the electrodes, which produce a high rate of secondary electron emission and field emission, we suggested a charge injector in dielectric barrier discharge. If the discharge gap is below 1 mm a high local electric field around sharp-end pyramids allows for boosting the secondary electron emission effect. A methane conversion of 25% was achieved in pyramid electrode plasma as opposed to merely 16% with the flat electrode. In

the reactor with a pyramid electrode, ethylene selectivity ranged from 16% to 24%, whereas with the flat electrode reactor, it was only 8%–10%. Pyramid electrode plasma has a higher ethylene selectivity compared to flat electrode plasma, Pyramid electrode plasma generally has a greater production efficiency than flat electrode plasma, even though it requires more operational power. The ethylene selective plasma reactor described in this experiment offers limitless opportunities in the petrochemical industry in the future.

ACKNOWLEDGMENTS

This work is supported by the H2020 European Research Council (ERC) Synergy Grant “Surface-CONfined fast modulated Plasma for Process and Energy intensification” (SCOPE), from the European Commission, with Grant No. 810182.

CONFLICT OF INTEREST STATEMENT

The authors declare no conflict of interest.

DATA AVAILABILITY STATEMENT

The data that support the findings of this study are available from the corresponding author upon reasonable request.

ORCID

Nima Pourali  <http://orcid.org/0000-0002-0962-5926>

REFERENCES

- [1] G. E. Rodgers, *Traveling with the Atom: A Scientific Guide to Europe and Beyond*, Royal Society of Chemistry, United Kingdom, **2019**, p. 222.
- [2] F. S. Roberts, K. P. Kuhl, A. Nilsson, *Angew. Chem.* **2015**, *127*(17), 5268.
- [3] M. Sarafraz, F. Christo, N. Tran, L. Fulcheri, V. Hessel, *Int. J. Hydrogen Energy* **2022**.
- [4] C. Liu, T. Hammer, R. Mallinson, *Catal. Today* **2004**, *98*(4), VII.
- [5] M. O. Adebajo, *Green Chem.* **2007**, *9*(6), 526.
- [6] H. Song, J. Jarvis, S. Meng, H. Xu, Z. Li, W. Li, *Methane Activation and Utilization in the Petrochemical and Biofuel Industries*, Springer, Germany, **2022**, pp. 23–41.
- [7] T. Baba, A. Miyaji, *Catalysis and the Mechanism of Methane Conversion to Chemicals*, Springer, **2020**.
- [8] O. B. Ayodele, *Int. J. Hydrogen Energy* **2022**.
- [9] Z. Navas-Anguita, P. L. Cruz, M. Martin-Gamboa, D. Iribarren, J. Dufour, *Fuel* **2019**, *235* 1492.
- [10] L. Wang, Y. Yi, C. Wu, H. Guo, X. Tu, *Angew. Chem., Int. Ed.* **2017**, *56*(44), 13679.
- [11] Y. Tian, L. Piao, X. Chen, *Green Chem.* **2021**, *23*(10), 3526.
- [12] A. H. B. Mostaghimi, T. A. Al-Attas, M. G. Kibria, S. Siahrostami, *J. Mater. Chem. A* **2020**, *8*(31), 15575.
- [13] T. J. Lawton, A. C. Rosenzweig, *Curr. Opin. Chem. Biol.* **2016**, *35*, 142.
- [14] T. Nozaki, K. Okazaki, *Catal. Today* **2013**, *211*, 29.
- [15] P. Chawdhury, Y. Wang, D. Ray, S. Mathieu, N. Wang, J. Harding, F. Bin, X. Tu, C. Subrahmanyam, *Appl. Catal., B* **2021**, *284*, 119735.
- [16] N. Pourali, M. Vasilev, R. Abiev, E. V. Rebrov, *J. Phys. D: Appl. Phys.* **2022**, *55*(39), 395204.
- [17] J. Osorio-Tejada, K. van't Veer, N. V. D. Long, N. N. Tran, L. Fulcheri, B. S. Patil, A. Bogaerts, V. Hessel, *Energy Convers. Manage.* **2022**, *269*, 116095.
- [18] N. Pourali, V. Hessel, E. V. Rebrov, *Plasma Chem. Plasma Process.* **2022**, *42*, 619.
- [19] N. Pourali, M. Sarafraz, V. Hessel, E. Rebrov, *Phys. Plasmas* **2021**, *28*(1), 013502.
- [20] N. Pourali, K. Lai, J. Gregory, Y. Gong, V. Hessel, E. V. Rebrov, *Plasma Processes Polym.* **2023**, *20*(1), 2200086.
- [21] O. Khalifeh, H. Taghvaei, A. Mosallanejad, M. R. Rahimpour, A. Shariati, *Chem. Eng. J.* **2016**, *294* 132.
- [22] C. -j. Liu, R. Mallinson, L. Lobban, *J. Catal.* **1998**, *179*(1), 326.
- [23] P. Lamichhane, T. R. Acharya, N. Kaushik, L. N. Nguyen, J. S. Lim, V. Hessel, N. K. Kaushik, E. H. Choi, *J. Environ. Chem. Eng.* **2022**, *10*(3), 107782.
- [24] A. Chehrghani, M. Torkamany, *Opt. Lasers Eng.* **2013**, *51*(1), 61.
- [25] T. Nozaki, Y. Unno, Y. Miyazaki, K. Okazaki, *J. Phys. D: Appl. Phys.* **2001**, *34*(16), 2504.
- [26] A. Mohanta, B. Lanfant, M. Leparoux, *Plasma Chem. Plasma Process.* **2019**, *39*(5), 1161.
- [27] R. W. B. Pearse, A. G. Gaydon, R. W. B. Pearse, A. G. Gaydon, *The Identification of Molecular Spectra*, Vol. 297, Chapman and Hall, London, **1976**.
- [28] M. Scapinello, E. Delikonstantis, G. D. Stefanidis, *Chem. Eng. Process.: Process Intensif.* **2017**, *117*, 120.
- [29] S. Heijkers, M. Aghaei, A. Bogaerts, *J. Phys. Chem. C Nanomater. Interfaces* **2020**, *124*(13), 7016.

How to cite this article: N. Pourali, P. Lamichhane, V. Hessel, E. V. Rebrov, *Plasma. Process. Polym.* **2023**, e2300007.
<https://doi.org/10.1002/ppap.202300007>